ACSNANO

www.acsnano.org

ARTICLE

A Monotargeting Peptidic Network Antibody Inhibits More Receptors for Anti-Angiogenesis

Kuo Zhang,[#] Hui Zhang,[#] Yong-Hong Gao,[#] Jia-Qi Wang, Yuan Li, Hui Cao,* Ying Hu,* and Lei Wang*

Cite This: *ACS Nano* 2021, 15, 13065−13076

Read Online

ACCESS | Metrics & More | Article Recommendations | Supporting Information

ABSTRACT: **The overexpression of growth factors and receptors on neovascular endothelial cells (ECs) and their binding may promote the abnormal growth of new blood vessels, leading to corneal neovascularization (CNV). Normally, monoclonal antibodies may bind and block only one growth factor or receptor, such as bevacizumab binding and blocking vascular endothelial growth factor (VEGF). Herein, we develop a monotargeting peptidic network antibody (pepnetibody) that blocks multiple receptors on the membrane of ECs through forming a fibrous network and ultimately achieves high-efficient treatment of CNV. The pepnetibody could bind to integrin $\alpha_v\beta_3$ in particulate formulation and *in situ* fibrillogenesis on ECs, mimicking the process of fibronectin fibrillogenesis on the cell membrane. The *in situ* formed peptidic network could firmly block integrin and cover other angiogenesis-related receptors, such as VEGF receptor-2 and neuropilin-1, exhibiting competitive efficacy of antiangiogenesis compared with traditional monoclonal antibody bevacizumab with 97.7 times lower dose.**

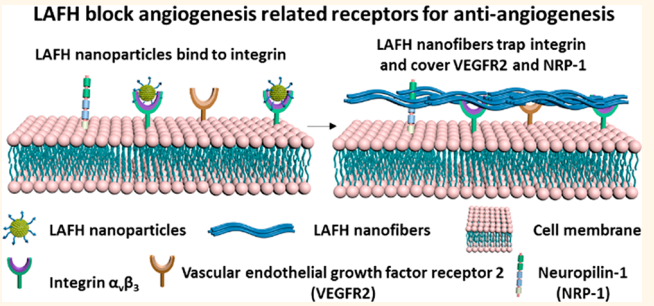

KEYWORDS: *peptidic network antibody, self-assembly, biomimetic, antiangiogenesis, corneal neovascularization*

Angiogenesis, a complex process of new capillary formation from existing blood vessels, is mainly regulated by a variety of growth factors and multiple signaling pathways.[1,2] The occurrence of angiogenesis, which is originated from the disruption of the dynamic balance between pro-angiogenesis and anti-angiogenesis under physiological conditions, is usually accompanied by a variety of diseases, such as eye diseases, tumors, and Parkinson's and Alzheimer's disease.[3]

Corneal neovascularization (CNV), the formation of new blood vessels in the avascular corneal tissue, is a pathological change of a variety of ocular surface disorders.[4,5] The angiogenesis seriously affects the transparency of the cornea, which eventually leads to the destruction of ocular tissue structure and damage of visual function. CNV has been identified to be a common factor in blindness and remains a huge challenge to cure clinically.[6]

Monoclonal antibodies have been used for the therapy of angiogenesis-related diseases, aiming to bind to vascular endothelial growth factor (VEGF) and inhibit the binding between VEGF and its receptors and the subsequent signaling pathway. For examples, ranibizumab and bevacizumab could be utilized for the treatment of CNV.[7] However, many growth factors, such as placenta growth factor 2, and many receptors, such as neuropilin-1 (NRP-1) and integrin, as well as the binding-induced signaling pathways, are responsible for the activation of angiogenesis. It is difficult for one monoclonal antibody to inhibit all binding processes between different kinds of growth factors and receptors.[8]

Supramolecular assembly strategies have been widely used for disease therapeutics.[9−14] Supramolecular structures could lead to improved efficacy and reduced side-effects.[15−18] Especially, the binding-induced fibrillogenesis (BIF) peptide that mimics fibrillogenesis of laminin or fibronectin during the formation of the natural extracellular matrix (ECM) to form fibrous networks on cell surfaces through binding receptors has drawn great attention.[19−22] The fibrous networks formed as an artificial ECM on the surface of cells cover cells and modulate the communication between the cells and the ECM. Therefore, the BIF peptide may bind a specific receptor to form a fibrous network on the surface of endothelial cells (ECs), further

Received: March 13, 2021
Accepted: July 26, 2021
Published: July 29, 2021

Scheme 1. (a) Molecular structure of LAFH and a cartoon of LAFH nanoparticles. (b) Schematic illustration of LAFH nanoparticles binding to integrin $\alpha_v\beta_3$ on the surface of ECs to form LAFH nanofibers, trapping integrin $\alpha_v\beta_3$ and covering other angiogenesis-related receptors (vascular endothelial growth factor receptor 2 and neuropilin-1) for the inhibition of neovascularization in a CNV rabbit model.

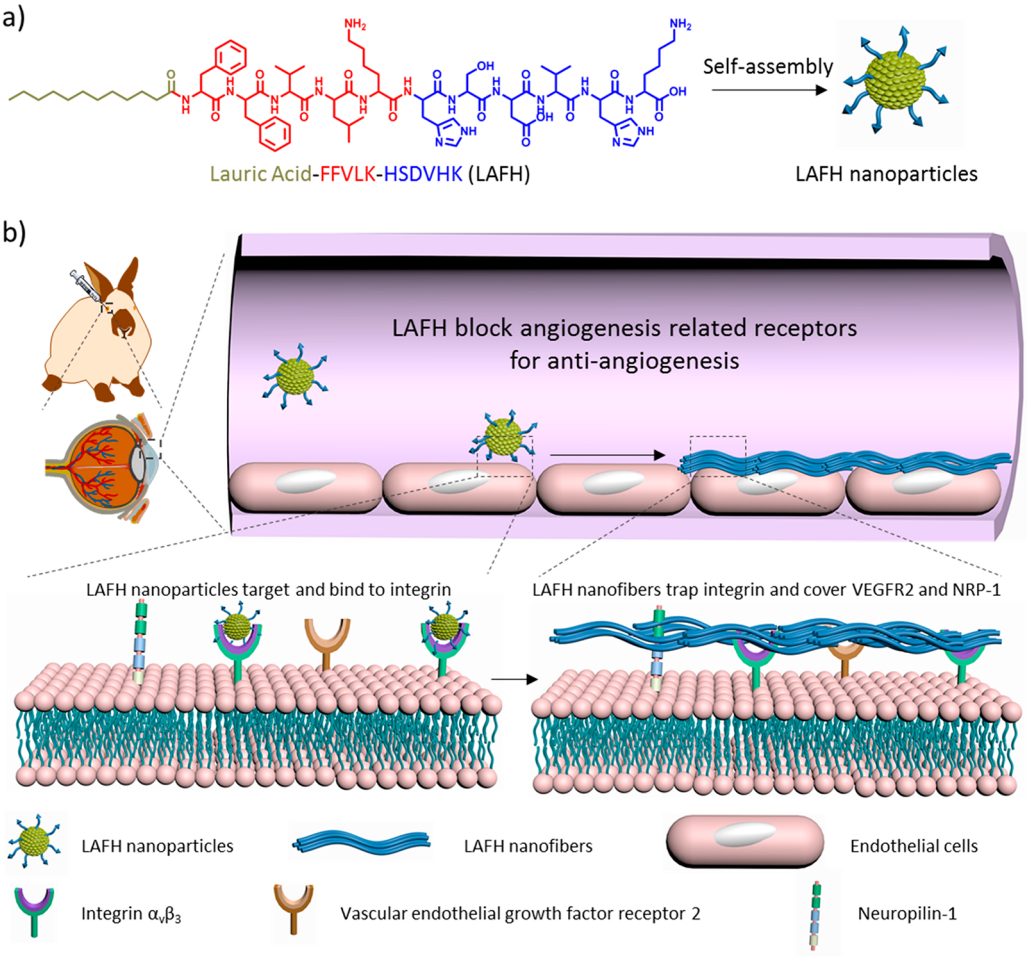

covering other angiogenesis-related receptors for highly efficient antiangiogenesis therapy.

Integrin $\alpha_v\beta_3$ is a kind of transmembrane glycoprotein, which could participate in mediating the interaction between cells and the ECM as a receptor.[23,24] Integrin provides attachment sites for cell adhesion and regulates migration, proliferation, and apoptosis of ECs.[25] Previous studies confirmed that blocking integrin-mediated cell-matrix interactions by BIF peptide could inhibit the migration and proliferation of vascular ECs, which ultimately inhibits angiogenesis.[26,27]

Herein, integrin $\alpha_v\beta_3$ was selected as a targeting receptor, and the BIF peptide was utilized to bind specifically to integrin $\alpha_v\beta_3$ on the surface of ECs to form a fibrous network for continuous trapping of integrin and covering other angiogenesis receptors, *i.e.*, VEGF receptor-2 (VEGFR2) and NRP-1, for the inhibition of CNV (Scheme 1). The BIF peptide was designed as lauric acid-FFVLK-HSDVHK (LAFH), which could bind to integrin $\alpha_v\beta_3$ through the HSDVHK sequence followed by forming a fibrous network through self-assembly of the KLVFF sequence on the membrane of ECs and inhibit the migration of ECs *in vitro*. The subconjunctival injection of LAFH into a CNV rabbit model allowed the formation of fibrous networks on ECs *in vivo*, not only trapping integrin $\alpha_v\beta_3$ but also covering other angiogenesis-related receptors, such as VEGFR2 and NRP-1. Therefore, the monotargeting LAFH (1.16 μg/kg) exhibited a similar antiangiogenesis effect against CNV to the monoclonal antibody bevacizumab (113.3 μg/kg) with a 97.7 times lower dose. Compared with the monoclonal antibody, the BIF peptide with antibody features was named peptidic network antibody (pepnetibody), showing great potential for antiangiogenesis.

RESULTS AND DISCUSSION

Design and Fibrillogenesis of LAFH. LAFH consists of three building blocks: (i) hydrophobic lauric acid, (ii) the hydrogen-bonding sequence KLVFF, and (iii) the integrin $\alpha_v\beta_3$ targeting sequence HSDVHK.[28,29] LAFH was purchased from GL Biochem, purified with liquid chromatography, and further characterized by electrospray ionization mass spectrometer mass spectra (ESI-MS) (Figures 1a and S1).

LAFH monomers could self-assemble into nanoparticles (NPs) in aqueous solution due to the hydrophobic dodecyl chain, the morphology of which was characterized through transmission electron microscopy (TEM). It was confirmed that LAFH, with a spherical morphology, exhibited an average diameter of 67.7 ± 11.1 nm. $CaCl_2$ was utilized as a simplified integrin $\alpha_v\beta_3$ for investigating the fibrillogenesis process of LAFH; the nature of binding between integrin and fibronectin is that Ca^{2+} in integrin binds to carboxyl in fibronectin.[30−32] The

https://doi.org/10.1021/acsnano.1c02194
ACS Nano 2021, 15, 13065−13076

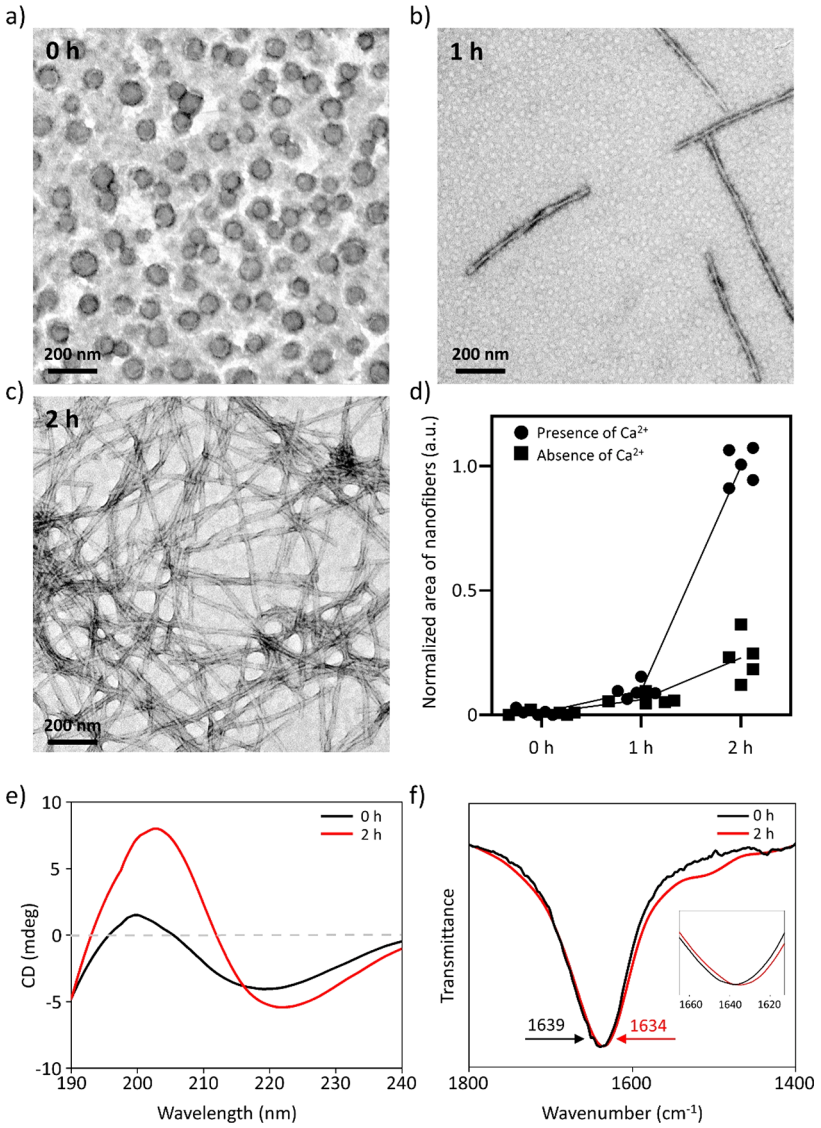

Figure 1. LAFH nanoparticles bind to Ca^{2+} and transform into nanofibers with β-sheet structures. (a–c) TEM images of LAFH nanoparticles incubated with $CaCl_2$ at 0 h with a spherical morphology (a), 1 h with both spherical and fibrous morphologies (b), and 2 h with a fibrous morphology (c). (d) Quantitative analysis of a normalized area of nanofibers from TEM images of LAFH nanoparticles incubated with/without $CaCl_2$, suggesting binding-induced fibrillogenesis. (e) CD and (f) FT-IR spectra of LAFH nanoparticles incubated with $CaCl_2$ at 0 and 2 h, indicating the formation of a β-sheet structure.

morphology of LAFH changed from NPs to an NP/nanofiber (NF) mixture after incubating with Ca^{2+} for 1 h and ultimately to NFs with average diameter of 18.7 ± 4.5 nm in 2 h (Figure 1a–c). The morphology of LAFH without Ca^{2+} could partially transform from NPs into NFs in 2 h. However, a particulate morphology could still be observed in the meantime (Figure S2a–c). The amount of NFs in TEM images was quantitatively analyzed, and it was found that the amount of LAFH NFs in the Ca^{2+} incubation group at 2 h was 4.3 times higher than that of the group in the absence of Ca^{2+}, which was calculated through the area of the NFs in the TEM images (Figure 1d). Therefore, it was validated that the binding between LAFH and Ca^{2+} accelerated the fibrillogenesis of LAFH NPs. TEM images also revealed that LAFH NPs without Ca^{2+} basically transformed into NFs in 4 h (Figure S2d). In addition, Na^+ cations were also introduced to validate the specificity of the fibrillogenesis of LAFH to Ca^{2+}. TEM results suggested that LAFH NPs could transform into NFs in 4 h (Figure S3), which was similar to LAFH alone. The phenomena indicated that the fibrillogenesis of LAFH could not be accelerated by Na^+ cations. The circular dichroism (CD) and Fourier transform infrared spectroscopy (FT-IR) spectra were measured to confirm the secondary structure of LAFH peptides in the form of NPs and NFs, respectively. LAFH NPs could form a typical spectrum of a β-sheet structure with a positive signal at 197 nm and a negative signal at 218 nm due to hydrogen bonds of KLVFF motifs, and the signal significantly increased after incubating with Ca^{2+} for 2 h (Figure 1e), which was in agreement with the formation of a mountain of NFs.[33] The LAFH NPs without incubation of Ca^{2+} showed a similar trend but a weak increase of peak intensities in the CD spectrum (Figure S2e), indicating the formation of a small amount of β-sheet-structured NFs. Moreover, the more detailed packing structure of LAFH was characterized by FT-IR. The peak presenting C═O stretching moved from 1639 cm^{-1} to 1634 cm^{-1} in the FT-IR spectra, also suggesting the formation of β-sheet-structured LAFH NFs by the stacking of LAFH during

https://doi.org/10.1021/acsnano.1c02194
ACS Nano 2021, 15, 13065–13076

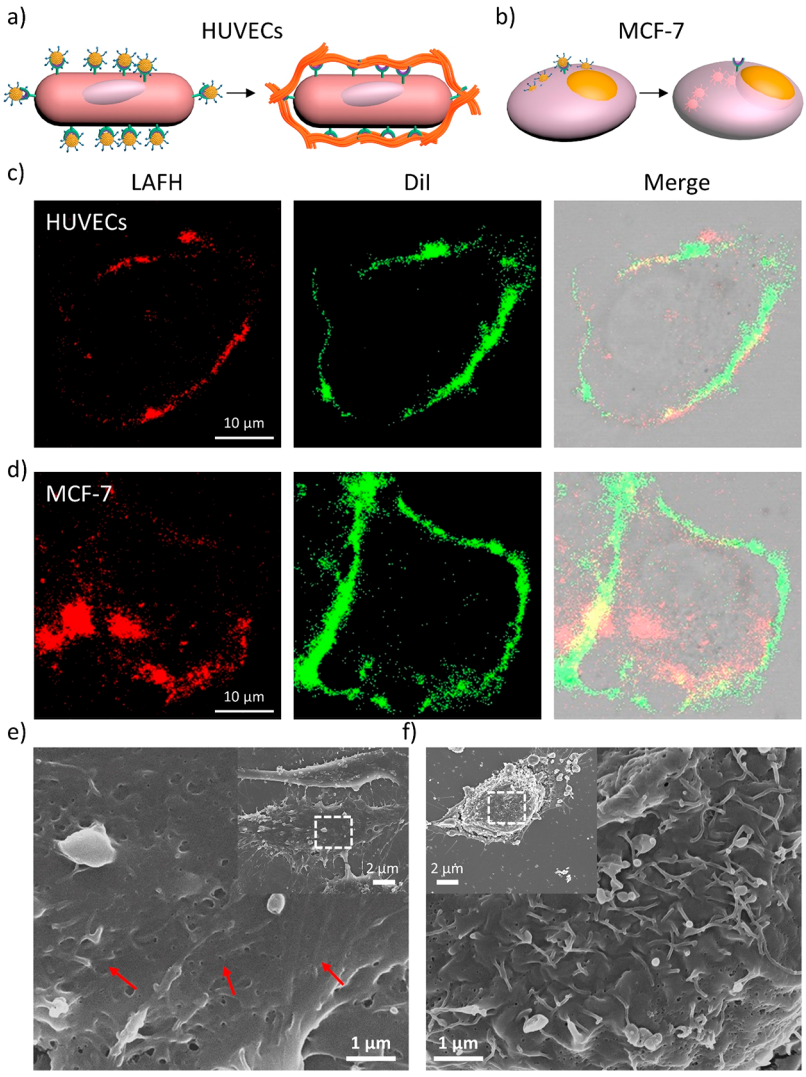

Figure 2. LAFH nanoparticles bind integrin $\alpha_v\beta_3$ and transform into nanofibers on HUVECs. (a) Schematic illustration of the formation of LAFH nanofibers on the surface of HUVECs induced by binding to integrin $\alpha_v\beta_3$. (b) Schematic illustration of the internalization of LAFH nanoparticles into MCF-7 cells. (c, d) CLSM images of HUVECs (c) and MCF-7 cells (d) incubated with Cy5-labeled LAFH nanoparticles for 2 h and stained with the membrane probe DiI for 10 min, indicating LAFH on the surface of HUVECs but inside MCF-7 cells, respectively. Green fluorescence signal represents the membrane probe and the red fluorescence signal shows Cy5-labeled LAFH. (e, f) SEM images of HUVECs treated with LAFH NPs (e) and PBS (f) to observe fibrous networks on the surface of HUVECs as indicated by red arrows.

the incubation with Ca^{2+} (Figure 1f).[34] Similar to the CD spectra, the LAFH lacking Ca^{2+} showed a relatively weak shift of peak position in the FT-IR spectra (Figure S2f).

LAFH NPs Bind to Integrin $\alpha_v\beta_3$ and Transform into NFs on HUVECs. The targeting ability of LAFH to integrin $\alpha_v\beta_3$ on cell membranes and the following fibrillogenesis were validated. Human umbilical vein endothelial cells (HUVECs) with overexpression of integrin $\alpha_v\beta_3$ were chosen as a positive experimental group, and MCF-7 cells were selected as a negative control.[35,36] The cell viability of HUVECs and MCF-7 cells incubated with LAFH NPs was tested by a cell counting kit-8 (CCK-8) assay, and the results showed that LAFH with a concentration of up to 80 μM exhibited negligible cytotoxicity to these cells after incubation for 24 h (Figure S4). The Cy5-labeled LAFH NPs were incubated with HUVECs or MCF-7 cells for 2 h (Figure 2a and b) followed by membrane staining with DiI for 10 min and observed by confocal laser scanning microscopy (CLSM). As shown in Figure 2c, red fluorescence was colocalized with green fluorescence of the membrane probe DiI on the surface of HUVECs, indicating the coverage of HUVECs by LAFH. In contrast, the red fluorescence signal was mainly located inside MCF-7 cells incubated with LAFH NPs, which can be attributed to the internalization of LAFH NPs (Figure 2d). Scanning electron microscopy (SEM) images provided direct evidence of the fibrillogenesis of LAFH NPs on HUVECs. Fibrous structures could be observed on the surface of HUVECs treated with LAFH NPs. In contrast, there were some wrinkles on the surface of PBS-treated HUVECs (Figure 2e and f). In addition, the surface of MCF-7 cells treated with LAFH NPs showed a large amount of irregular protrusions, which was similar to the PBS-treated cells (Figure S5). These results validated that LAFH NPs could bind to $\alpha_v\beta_3$ and form fibrous networks on the surface of HUVECs, not MCF-7 cells, indicating that the overexpression of $\alpha_v\beta_3$ on the cell surface was crucial for the fibrillogenesis of LAFH NPs.

LAFH Inhibits the Migration of HUVECs *in Vitro*. The LAFH fibrous network on HUVECs was expected to bind and block $\alpha_v\beta_3$, resulting in the inhibition of HUVEC migration. The

https://doi.org/10.1021/acsnano.1c02194
ACS Nano 2021, 15, 13065−13076

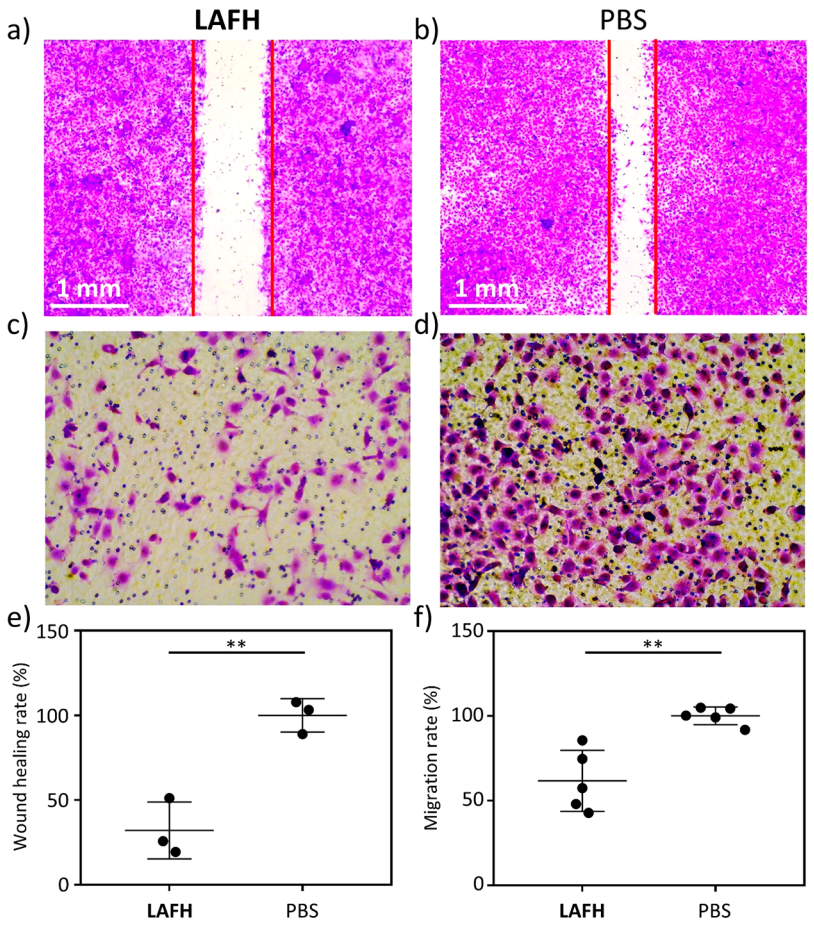

Figure 3. LAFH nanoparticles inhibit migration of HUVECs. (a, b) Microscopy image of a wound healing experiment of HUVECs treated with LAFH NPs (a) or PBS (b). White areas indicate no migrated cells. (c, d) Microscopy images of migrated HUVECs treated with LAFH NPs (c) or PBS (d) in a Transwell migration assay. Purple areas indicate migrated cells. (e) Quantitative analysis of the wound healing rate in (a) and (b), suggesting the migration inhibition of HUVECs by LAFH. (f) Quantitative analysis of the migration rate in (c) and (d), indicating the migration inhibition of HUVECs by LAFH.

wound healing experiment was carried out to evaluate the anti-angiogenesis effect of LAFH. The wound healing area in LAFH NPs-treated HUVECs was significantly smaller ($n = 3$, $p < 0.01$, Student's t-test) than that of the PBS group (Figure 3a, b, and e). No significant difference in the area of wound healing was observed between LAFH- and PBS-treated MCF-7 cells (Figure S6a, b and e). Furthermore, a Transwell migration experiment was also performed to confirm the inhibition effect of cell migration by LAFH. It was clear that LAFH NPs-treated HUVCEs showed a lower migration rate than that of the PBS group, which was calculated based on the number of migrated cells ($n = 5$, $p < 0.01$, Student's t-test) (Figure 3c, d, and f). In addition, there was almost no difference in the migration rate between LAFH NPs- and PBS-treated MCF-7 cells (Figure S6c, d, and f). The evidence indicated that the formed LAFH NFs on the surface could trap overexpressed integrin $\alpha_v\beta_3$ and thus inhibit the migration of HUVECs. In the meantime, internalized LAFH NPs exhibited a negligible effect on the migration inhibition of MCF-7 cells with less expressed integrin $\alpha_v\beta_3$.

LAFH NPs Transform into NFs and Trap Integrin $\alpha_v\beta_3$, which Inhibits the Migration of ECs in a CNV Rabbit Model *in Vivo*. The LAFH NPs could form fibrous networks on the surface of HUVECs through binding $\alpha_v\beta_3$, which may further trap integrin $\alpha_v\beta_3$ for the migration inhibition of ECs. In order to validate the hypothesis, we established a CNV rabbit model by using alkali to burn the rabbit's cornea (Figure 4a).[37] LAFH NPs (20 μM, 100 μL) and PBS (100 μL) were injected into the CNV rabbit on day 0 through subconjunctival injection (Figure 4a). The CNV sections were collected and fixed on day 7, followed by thioflavin T (ThT) staining and immunostaining of integrin $\alpha_v\beta_3$. ThT, which could emit a green fluorescence signal after insertion into a β-sheet structure, was used to stain *in situ* formed LAFH NFs.[38] As shown in Figure 4b and c, the green fluorescence of ThT in the CNV area of the LAFH NPs-treated rabbit was much higher than that of the PBS group 7 days after the injection, indicating the high accumulation and long-term retention of LAFH NFs (Figure 4d). TEM images of the corneal tissue showed a fibrous structure could be observed on the surface of ECs in the LAFH NPs-treated group rather than the PBS group (Figure 4e and f). These results validated the fibrillogenesis of LAFH NPs on ECs in the CNV area, which may result in the high accumulation and long-term retention of LAFH. In addition, it was found that the green fluorescence of ThT was well-colocalized with the red fluorescence of integrin $\alpha_v\beta_3$, indicating that the LAFH did bind to integrin $\alpha_v\beta_3$ (Figure 4g). However, the red fluorescence was weak, probably due to the trapping of integrin $\alpha_v\beta_3$ by LAFH NFs and the subsequent inhibition of integrin $\alpha_v\beta_3$ immunostaining by specific primary antibody and dye-labeled secondary antibody.

https://doi.org/10.1021/acsnano.1c02194
ACS Nano 2021, 15, 13065−13076

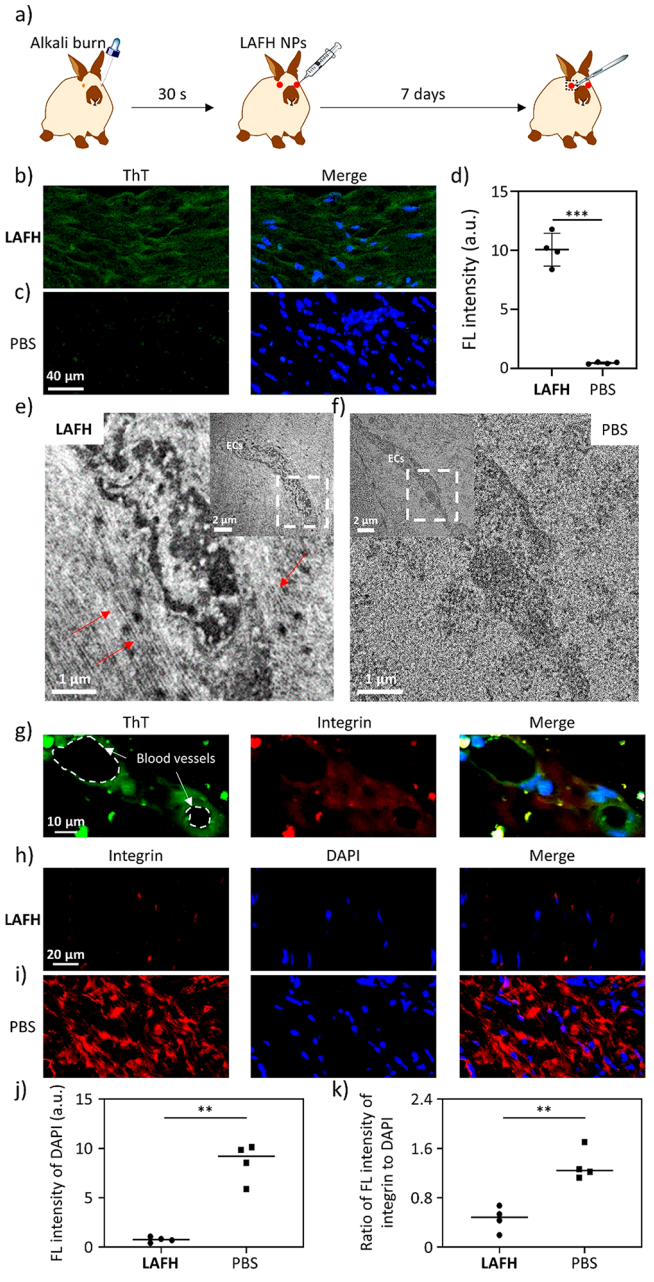

Figure 4. Fibrillogenesis of LAFH traps $\alpha_v\beta_3$, which inhibits the migration of ECs in a CNV rabbit model *in vivo*. (a) Schematic illustration for the establishment of a CNV rabbit model and the following treatment of LAFH NPs. (b, c) Fluorescence and immunofluorescence images of the fluorescence signal of the CNV area after injection of LAFH NPs (b) or PBS (c) for 1 week. Green signal for ThT and blue signal for DAPI. (d) Quantitative analysis of the intensity of the green fluorescence signal in (b) and (c), suggesting the high accumulation and long-term retention of LAFH. (e, f) TEM images of the CNV area after injection of LAFH NPs for 1 week to show NFs around ECs (e, red arrows) and no fibrous structure in the PBS group (f). (g) Fluorescence images of LAFH (ThT, green), integrin $\alpha_v\beta_3$ (red), and nucleus (blue) to show the colocalization of LAFH and integrin $\alpha_v\beta_3$. (h, i) Immunofluorescence images of integrin in the CNV area after injection of LAFH NPs (h) or PBS (i) for 1 week. Red signal for integrin $\alpha_v\beta_3$ and blue signal for DAPI. (j, k) Quantitative analysis of DAPI (j) and ratio of fluorescence intensity of integrin to DAPI (k) from both (h) and (i), indicating fewer migrated cells and less detected integrin $\alpha_v\beta_3$ due to the trapping of LAFH NFs.

The blue fluorescence signal of DAPI in the CNV area of the LAFH group was lower than that of the PBS group (Figure 4h, i, and j, $n = 4$, $p < 0.01$, Student's *t*-test), suggesting the migration inhibition effect of ECs by LAFH NFs. Therefore, it was reasonable that the amount of integrin $\alpha_v\beta_3$ in the CNV area detected through the red fluorescence signal was lower than that of the PBS group (Figure 4h and i) due to fewer ECs. In order to evaluate the binding and trapping ability of LAFH to integrin $\alpha_v\beta_3$ by fibrillogenesis on EC surfaces, we calculated the ratio of fluorescence intensity of integrin $\alpha_v\beta_3$ (red) to DAPI (blue). It was found that the ratio of integrin $\alpha_v\beta_3$ to DAPI of the LAFH NPs-treated group was lower than that of the PBS group (Figure 4h, i, and k, $n = 4$, $p < 0.01$, Student's *t*-test), which revealed that the immunostaining of integrin $\alpha_v\beta_3$ by primary antibody and subsequent dye-labeled secondary antibody was inhibited. These results indicated the highly efficient binding and trapping of integrin $\alpha_v\beta_3$ through fibrillogenesis of LAFH.

LAFH NFs Cover Angiogenesis-Related VEFGR2 and NRP-1 *in Vivo*. We hypothesized that the LAFH fibrous networks on the cell surface may cover other angiogenesis-related receptors. Therefore, we immunostained typical VEGFR2 (Figure 5a and b) and NRP-1 (Figure 5e and f) and evaluated the coverage of these receptors by LAFH NFs. The ratio of receptors (red) to ECs (blue) in the CNV region was quantitatively analyzed (Figure 5c and g). The results exhibited the ratio of red to blue fluorescence signal in the LAFH group was lower than that of the PBS group ($n = 4$, $p < 0.05$, Student's *t*-test), indicating that VEGFR2 (Figure 5c) and NRP-1 (Figure 5g) were less recognized and bound by specific primary antibodies and subsequent dye-labeled secondary antibodies due to the coverage by LAFH fibrous networks on the cell surfaces. This evidence suggested that LAFH NFs could not only trap $\alpha_v\beta_3$ but also cover other receptors, *i.e.*, VEGFR2 and NRP-1. Meanwhile, the decrease of blue fluorescence intensity (Figure 5d and h, $n = 4$, $p < 0.01$, Student's *t*-test) in the LAFH group compared with the PBS group validated that LAFH inhibited the migration of ECs.

The CNV area of rabbits receiving two injections (day 0 and 7) was further evaluated on day 14. The fluorescence intensity of ThT in the LAFH NPs-treated group was still higher than that of the PBS group (Figure S7a–c) ($n = 4$, $p < 0.001$, Student's *t*-test). In addition, the difference of ThT fluorescence between the LAFH and PBS group in 2 weeks (Figure S7c) was 13.0 times higher than that in 1 week (Figure 4d). The increase of ThT fluorescence indicated that the existing LAFH NFs could promote further accumulation of subsequent LAFH NPs in the CNV area, possibly beneficial for long-term therapy of CNV. Similar decreases in the ratio of integrin $\alpha_v\beta_3$ to cells in the CNV area ($n = 4$, $p < 0.01$, Student's *t*-test) in the LAFH group compared with the PBS group were observed (Figure S7d and e), suggesting continuous trapping of integrin $\alpha_v\beta_3$ by LAFH NFs. The trapping of integrin $\alpha_v\beta_3$ in 2 weeks was even better than that in 1 week because the difference between PBS and LAFH groups of integrin $\alpha_v\beta_3$ to DAPI in 2 weeks was 1.3 times higher than that in 1 week (Figures 4k and S7g). However, no significant difference was observed in the amount of blue signal, indicating no significant difference in the amount of ECs in the LAFH NPs- and PBS-treated group after 2 weeks (Figure S7f). The amount of VEGFR2 (Figure S8a–d) and NRP-1 (Figure S8e–h) was also lower in the LAFH NPs-treated group comparing with the PBS-treated group, indicating that these receptors were still covered by LAFH NFs. In order to exclude the mechanism in which LAFH NFs inhibit the expression of

https://doi.org/10.1021/acsnano.1c02194
ACS Nano 2021, 15, 13065–13076

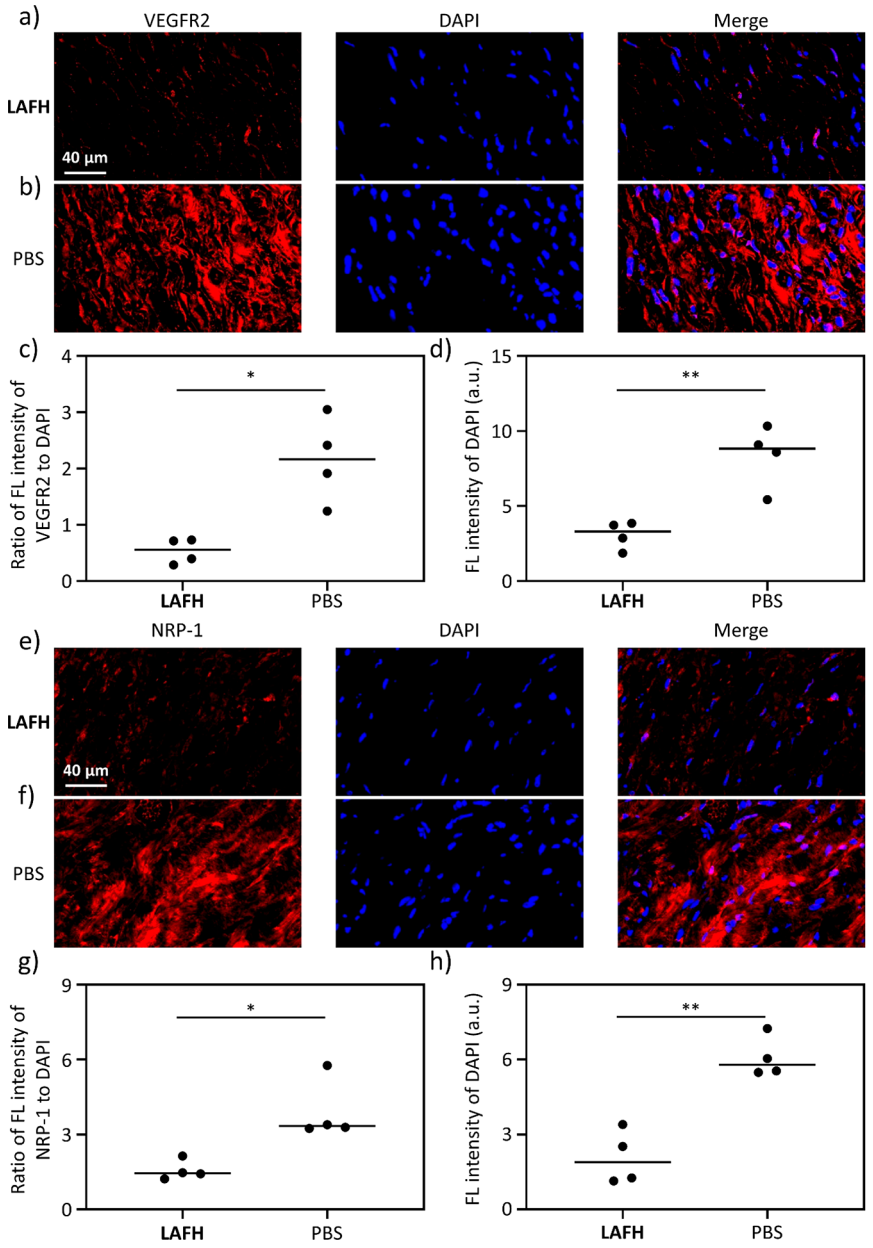

Figure 5. LAFH nanofibers on ECs block VEGFR2 and NRP-1. (a, b) Immunofluorescence images of VEGFR2 in the CNV area after injection of LAFH NPs (a) or PBS (b) for 1 week. Red signal for VEGFR2 and blue signal for DAPI. (c) Quantitative analysis of the ratio of fluorescence intensity of VEGFR2 to DAPI in (a) and (b) suggesting the coverage of VEGFR2 by LAFH NFs. (d) Quantitative analysis of the fluorescence intensity of DAPI indicating the migration inhibition of ECs in (a) and (b). (e, f) Immunofluorescence images of NRP-1 in the CNV area after injection of LAFH NPs (e) or PBS (f) for 1 week. Red signal for NRP-1 and blue signal for DAPI. (g) Quantitative analysis of the ratio of fluorescence intensity of NRP-1 to DAPI in (e) and (f) suggesting the coverage of NRP-1 by LAFH NFs. (h) Quantitative analysis of the fluorescence intensity of DAPI (h) indicating the migration inhibition of ECs in (e) and (f).

receptors, the expression of VEGFR2 and NRP-1 on HUVECs treated with LAFH NPs was measured by Western blot. As shown in Figure S9, both VEGFR2 and NRP-1 were expressed on LAFH NPs-treated HUVECs, the amount of which exhibited a negligible difference compared with PBS-treated HUVECs. This evidence suggested that the coverage of LAFH did not inhibit the expression of angiogenesis-related receptors, *i.e.*, VEGFR2 and NRP-1. The LAFH may achieve an anti-angiogenesis effect through blocking the angiogenesis-related signaling pathway rather than inhibiting the expression of related receptors.

LAFH Inhibits Angiogenesis in a CNV Rabbit Model. The anti-angiogenesis effect of LAFH in a CNV rabbit model was finally examined, and the clinical monoclonal antibody bevacizumab was used as a positive control. The pictures of rabbit eyes treated with LAFH NPs, bevacizumab, and PBS for 1 week (Figure 6a–c) are presented, respectively. It was found that both average length (Figure 6d, $p < 0.001$, Student's t-test) and area (Figure 6e, $p < 0.01$, Student's t-test) of the CNV region in the LAFH and bevacizumab groups were significantly lower than the PBS group, indicating the excellent and similar antiangiogenesis effect of both the LAFH and bevacizumab groups ($n = 8$). The hematoxylin–eosin (H&E) staining was

https://doi.org/10.1021/acsnano.1c02194
ACS Nano 2021, 15, 13065–13076

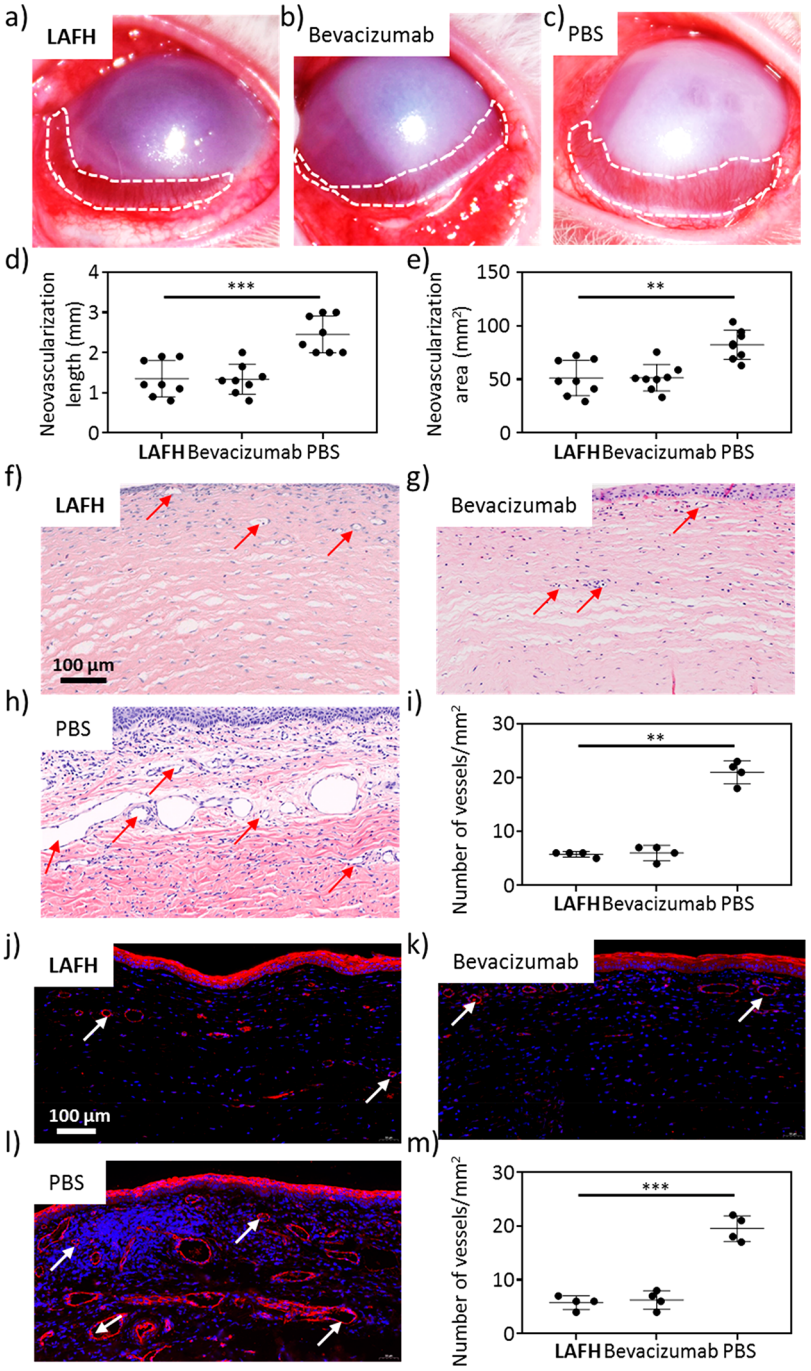

Figure 6. LAFH inhibits angiogenesis in a CNV rabbit model *in vivo*. (a–c) Photo of eyes in the CNV rabbit model treated with LAFH NPs (a), bevacizumab (b), and PBS (c) for 1 week, respectively. White dashed line shows neovascularization in the CNV area. (d, e) Quantitative analysis in the length (d) and area (e) of neovascularization in the CNV area, indicating the therapeutic effect of LAFH NPs and bevacizumab on CNV compared with the PBS group. (f–h) H&E staining of the eye cup in the CNV rabbit model on day 7 after treatment with LAFH NPs (f), bevacizumab (g), and PBS (h). Red arrows show newly formed blood vessels. (i) Quantitative analysis of the number of newly formed blood vessels in (f)–(h), indicating less angiogenesis formed after treatment with LAFH or bevacizumab. (j–l) Immunofluorescence images for CD31 of the CNV area in the LAFH NPs- (j), bevacizumab- (k), or PBS- (l) treated CNV rabbit for 1 week. White arrows indicate newly formed blood vessels. (m) Quantitative analysis on the number of newly formed blood vessels in (j)–(l), suggesting less angiogenesis after treatment by LAFH or bevacizumab.

also performed for validating the antiangiogenesis effect of LAFH in the CNV rabbit model. The number of newly formed blood vessels (red arrows) of LAFH- (Figure 6f) and bevacizumab- (Figure 6g) treated groups were similar to each other, but significantly lower than the PBS-treated group (Figure 6h) for 1 week (Figure 6i, $n = 4$, $p < 0.01$, Student's t-test). A marker of newly formed blood vessels, CD31, was used to stain the CNV area. The immunofluorescence staining images (Figure 6j–l) showed a smaller number of newly formed blood vessels in the LAFH and bevacizumab groups than that of the PBS group ($n = 4$, $p < 0.001$, Student's t-test), which was consistent with the result of H&E staining (Figure 6m). These

https://doi.org/10.1021/acsnano.1c02194
ACS Nano 2021, 15, 13065–13076

powerful evidences suggested that the antiangiogenesis effect of LAFH was comparable to bevacizumab. Furthermore, the CNV rabbits receiving two injections, on day 0 and 7, were characterized on day 14. The CNV in the rabbit progressed over time, and LAFH and bevacizumab still exhibited similar therapeutic effects (Figure S10). Notably, even though LAFH and bevacizumab shared the same molar concentration (20 μM, 100 μL), the dose of LAFH (1.16 μg/kg) was significantly lower than that of bevacizumab (113.3 μg/kg), which indicated the high therapeutic efficacy of LAFH as a pepnetibody compared with the monoclonal antibody bevacizumab. Monotargeting LAFH NFs trap and cover angiogenesis-related receptors for highly efficient treatment of multi-pathway-triggered angiogenesis.

CONCLUSIONS

In summary, we designed a BIF peptide, LAFH, as a pepnetibody for antiangiogenesis through inhibiting angiogenesis-related receptors. The LAFH NPs could bind to integrin $\alpha_v\beta_3$ and form a fibrous network through mimicking the fibronectin fibrillogenesis in the ECM, *i.e.*, binding-induced fibrillogenesis, resulting in the blockage of the integrin $\alpha_v\beta_3$ on cell membranes and further migration inhibition of integrin $\alpha_v\beta_3$-overexpressing HUVECs *in vitro*. The LAFH fibrous network was formed and colocalized with integrin $\alpha_v\beta_3$ on the membrane of ECs for trapping integrin $\alpha_v\beta_3$ after subconjunctival injection in a CNV rabbit model. In addition, other receptors related to angiogenesis, such as VEGFR2 and NRP-1, were also covered by the LAFH fibrous network, which may contribute to the high efficacy of anti-angiogenesis. LAFH exhibited an excellent therapeutic effect compared with the monoclonal antibody bevacizumab with a lower dose (97.7 times lower than bevacizumab), which could be utilized for the treatment of CNV and potentially other angiogenesis-related diseases.

We demonstrated that the BIF peptide as a pepnetibody could bind to the specific receptor and process fibrillogenesis on cell membranes with a multivalent effect. The fibrous network exhibited long-term retention on cell membranes rather than internalizing into cells, leading to a long-term therapeutic effect. The pepnetibody could not only bind to the targeting receptor but also cover other nontargeted receptors on the cell membranes, resulting in highly efficient therapy for multi-pathway-induced diseases. Other aspects of the pepnetibody, such as a bispecific targeting pepnetibody, are under investigation in our lab.

MATERIALS AND METHODS

Materials. All solvents were used without further purification. Dimethyl sulfoxide (DMSO), Cy5, and hexafluoroisopropanol were purchased from Aladdin. The CCK-8 was provided by Beyotime Institute of Biotechnology (Shanghai, China). HUVECs and MCF-7 cell lines were purchased from Cell Culture Center of Institute of Basic Medical Sciences, Chinese Academy of Medical Sciences (Beijing, China).

Preparation of Cy5-Labeled LAFH. For the preparation of Cy5-labeled LAFH, LAFH (4 mM in DMSO, 500 μL) was mixed with Cy5 (4 mM in DMSO, 50 μL). The pH value was adjusted to 9 with triethylamine. The solution was stirred in an ice bath overnight and was further dialyzed to remove free Cy5. The resultant solution was freeze-dried before being used.

Binding-Induced Fibrillogenesis in Solution and *in Vitro*. *Transmission Electron Microscope.* The measurements were performed on an HT-7700 TEM (Hitachi, Tokyo, Japan); 10 μL of LAFH (20 μM) in the presence or absence of Ca^{2+} (20 μM) was dropped on a copper mesh for 10 min. Then filter paper was used to remove excess solvent. The samples were dyed by 10 μL of phosphotungstic acid (2% wt in H_2O) for 5 min before being removed by filter paper. Finally, the copper mesh was cleaned with 10 μL of deionized water, then absorbed by filter paper and dried.

Circular Dichroism. The measurements were performed on a CD spectrometer (JASCO-1500, Tokyo, Japan). LAFH (20 μM in H_2O with 0.5% hexafluoroisopropanol in volume) with or without $CaCl_2$ (20 μM) was prepared and further stored at room temperature before testing. The measurements were performed between 190 and 240 nm with a resolution of 2.0 nm and a scanning speed of 500 nm/min.

Fourier Transform Infrared Spectroscopy. Measurements were performed on a spectrometer (SP-200i, PerkinElmer, USA) using KBr pellets. LAFH (20 μM in H_2O with 0.5% DMSO in volume) with or without $CaCl_2$ (20 μM) was prepared and further stored at room temperature. A 10 μL amount of the samples was dropped on the KBr pellet and dried. The measurements were performed between 4000 and 400 cm^{-1}.

Cytotoxicity Assay for HUVECs and MCF-7 Cells. The CCK-8 assay was employed to evaluate the cytotoxicity of HUVECs and MCF-7 cells treated with LAFH. The cells were precultured in 96-well plates for 24 h at a density of 6×10^3 cells per well. A series of different concentrations (10, 20, 40, 80, and 160 μM) of LAFH were added and co-incubated with cells in the medium for another 24 h. The medium was removed and washed with PBS three times. A 100 μL amount of the CCK-8 solutions (10% in medium) was added to each well and cultured for 2 h. The UV−vis absorption was measured by a multimode microplate detection system (Enspire, America) for each well at a test wavelength of 450 nm and a reference wavelength of 690 nm.

Confocal Laser Scanning Microscopy. CLSM characterization was performed on a Zeiss 710 scanning confocal microscope (Zeiss). HUVECs or MCF-7 cells were precultured in medium overnight, and after removal of the culture, the Cy5-labeled LAFH (40 μM, 0.5% DMSO in volume in serum-free medium) was co-incubated with HUVECs or MCF-7 cells for 2 h before CLSM observation. The fluorescence signal of Cy5 was collected at an excitation wavelength of λ_{ex} = 633 nm and λ_{em} = 662 nm with a red pseudocolor. The fluorescence signal of DiI was collected at an excitation wavelength of λ_{ex} = 549 nm and λ_{em} = 565 nm with pseudocolor of green.

Scanning Electron Microscopy. SEM was detected on a NOVA Nano 430 SEM (FEI). The LAFH NPs (20 μM in medium, 1 mL) were incubated with HUVECs or MCF-7 cells on a silicon wafer for 2 h, then fixed with paraformaldehyde (4% in PBS) for 1 h. These cells were further dehydrated with ethanol for 10 min for each gradient (volume ratio of alcohol to water: 10, 30, 50, 70, 90, and 100%) and *tert*-butanoluse for 10 min. Finally, the samples were further coated with gold before being photographed.

Migration Inhibition *in Vitro*. *Wound Healing Experiment.* HUVECs and MCF-7 cells (1×10^4 cells per well) were cultured with medium in a six-well plate for 24 h. The cell layers were scratched with a pipet tip to obtain a physical wound. The wells were washed three times with PBS after removing the medium. Then, the two kinds of cells were cultured with LAFH NPs (20 μM in medium) for 24 h. Paraformaldehyde (4% in PBS) was employed to fix cells for 10 min, which were subsequently stained with crystal violet (0.1 wt % in PBS) for 2 min. Finally, the samples were observed under a microscope. The wound healing rate was calculated as below: The healed area in the PBS group was normalized as 100%. The wound healing rate of the LAFH group was calculated as the healed area in the LAFH group divided by the healed area in the PBS group.

Transwell Migration Assay. HUVECs or MCF-7 cells were starved for 24 h and then digested with trypsin to obtain individual cells. LAFH cocultured with HUVECs and MCF-7 cells was set on the upper layer without fetal bovine serum (FBS). DMEM with FBS (10% in volume) was added to the lower layer of the chamber. The Transwell plates were incubated in an oven at 37 °C for 24 h. After fixing with paraformaldehyde (4% in PBS), the cells were further stained with crystal violet (0.1 wt % in PBS). The samples were washed with PBS three times and observed by a microscope.

https://doi.org/10.1021/acsnano.1c02194
ACS Nano 2021, 15, 13065−13076

Bioeffect of LAFH *in Vivo*. *Alkali-Induced Corneal Neovascularization.* Thirty healthy male New Zealand strain albino rabbits weighing from 2.4 to 3.3 kg were used in the project. Experimental procedures of all animals in this study were conducted according to the ARVO Statement for the Use of Animals in Ophthalmic and Vision Research and were approved by the Animal Care Committee of Shanghai Jiaotong University (No. TJHBLAC-200917), Shanghai, China. All experiments were executed on the *oculus dexter* (*OD*) eyes. Induction of CNV was carried out according to the previous method with some adjustment. Briefly, after the rabbits were anesthetized, a 5.5-mm-diameter round filter paper (type 3, Whatman Co., USA) was soaked in NaOH (1 M) for 60 s. The wet filter paper was transferred to the central cornea and maintained for 30 s. The corneal surface was immediately rinsed with physiological saline (60 mL) for more than 2 min. The rabbits were divided into three groups of 10 rabbits per group randomly: (1) The *OD* eye of each rabbit received subconjunctival injection (20 μM, on day 0 and 7) of PBS (Roche, USA); (2) the *OD* eye of each rabbit received subconjunctival injection (20 μM, on day 0 and 7) of LAFH NPs; (3) the *OD* eye of each rabbit received subconjunctival injection (20 μM, on day 0 and 7) of bevacizumab (Genentech/Novartis, South San Francisco, CA, USA).

Quantification of CNV. The CNV modeling day was considered as day 0. We assessed all eyes daily and revealed the development of CNV at the seventh and 14th day after alkaline cauterization by a slit-lamp (SL-120; Zeiss, Jena, Germany). The total area of CNV and the length of the longest CNV were quantified by ImageJ software (NIH) at the time points indicated. To examine neovascularization formation, the histopathological analysis and CD31+ (Santa Cruz, USA; 1:200) immunofluorescence (IF) staining were performed for the vascular system at different time points as described. The number of blood vessels was calculated blindly by two pathologists.

Immunofluorescence Staining. CNV tissues in different groups were collected and fixed in paraformaldehyde (4% in PBS buffer). The slices were sectioned after being embedded in paraffin and further deparaffinized through EDTA buffer under microwave. The slices were stained by ThT (Shanghai yuanye), followed by immunostaining with primary antibodies (anti-integrin $\alpha_v\beta_3$ antibody, bs-1310R, Bioss, China; anti-VEGFR2 antibody, ab233693, Abcam, China; anti-neuropilin-1 antibody, bs-10412R, Bioss, China) and subsequent dye-labeled secondary antibody (Cy3-conjugated goat anti-mouse/rabbit IgG (H+L), Beyotime, China), and were further observed with a Pannoramic MIDI digital slide scanner (3Dhistech).

Statistical Analysis. All data are reported as the means ± SD. The *in vitro* experiments were performed in three independent experiments with 3−5 technical replicates. The *in vivo* experiments were performed with 5 or 8 rabbits in each group. Statistical analysis of the samples was performed using unpaired two-tailed Student's *t*-test, and a p value of <0.05 was considered significant.

ASSOCIATED CONTENT

Supporting Information

The Supporting Information is available free of charge at https://pubs.acs.org/doi/10.1021/acsnano.1c02194.

ESI-MS and HPLC spectra of LAFH; morphology transformation of LAFH in the absence of Ca^{2+} in solution; morphology of LAFH in the presence of Na^+ in solution; cell cytotoxicity of LAFH on HUVECs and MCF-7 cells; SEM and cell migration experiments of LAFH on MCF-7 cells; *in vivo* experiments of LAFH on a CNV rabbit model after 2 weeks (PDF)

AUTHOR INFORMATION

Corresponding Authors

Hui Cao − *Department of Materials Physics and Chemistry, School of Materials Science and Engineering, University of Science and Technology Beijing, Beijing 100083, China;* orcid.org/0000-0001-8236-5350; Email: caohui@mater.ustb.edu.cn

Ying Hu − *Shanghai Jiao Tong University Affiliated Sixth People's Hospital, Shanghai 200233, China;* Email: 2238067351@qq.com

Lei Wang − *CAS Center for Excellence in Nanoscience, CAS Key Laboratory for Biomedical Effects of Nanomaterials and Nanosafety, National Center for Nanoscience and Technology (NCNST), Beijing 100190, China;* orcid.org/0000-0003-1405-9815; Email: wanglei@nanoctr.cn

Authors

Kuo Zhang − *Department of Materials Physics and Chemistry, School of Materials Science and Engineering, University of Science and Technology Beijing, Beijing 100083, China; CAS Center for Excellence in Nanoscience, CAS Key Laboratory for Biomedical Effects of Nanomaterials and Nanosafety, National Center for Nanoscience and Technology (NCNST), Beijing 100190, China;* orcid.org/0000-0003-3687-3172

Hui Zhang − *Shanghai Jiao Tong University School of Medicine, Shanghai 200025, China;* orcid.org/0000-0002-6478-1358

Yong-Hong Gao − *Department of Materials Physics and Chemistry, School of Materials Science and Engineering, University of Science and Technology Beijing, Beijing 100083, China; CAS Center for Excellence in Nanoscience, CAS Key Laboratory for Biomedical Effects of Nanomaterials and Nanosafety, National Center for Nanoscience and Technology (NCNST), Beijing 100190, China;* orcid.org/0000-0003-2575-7694

Jia-Qi Wang − *CAS Center for Excellence in Nanoscience, CAS Key Laboratory for Biomedical Effects of Nanomaterials and Nanosafety, National Center for Nanoscience and Technology (NCNST), Beijing 100190, China*

Yuan Li − *CAS Center for Excellence in Nanoscience, CAS Key Laboratory for Biomedical Effects of Nanomaterials and Nanosafety, National Center for Nanoscience and Technology (NCNST), Beijing 100190, China;* orcid.org/0000-0002-4588-8977

Complete contact information is available at: https://pubs.acs.org/10.1021/acsnano.1c02194

Author Contributions

#K.Z., H.Z., and Y.-H.G. contributed equally.

Author Contributions

L.W. and Y.H. conceived the project and designed the experiments. K.Z. and Y.-H.G performed the synthesis and characterization in solution and at the cellular level. J.-Q.W. and Y.L. assisted with the cellular studies. H.Z. performed the animal studies. H.C., L.W., and Y.H. supervised the project. L.W., K.Z., H.Z., Y.-H.G., and Y.H. wrote the manuscript.

Notes

The authors declare no competing financial interest.

ACKNOWLEDGMENTS

This work was supported by National Key R&D Program of China (No. 2018YFE0205400), National Natural Science Foundation of China (51890891, 52073027, 51773017, 51890894, 51725302, 21807020, 51573031, and 51573032), the Fundamental Research Funds for the Central Universities (No. FRF-DF-19-001), and CAS Interdisciplinary Innovation Team.

REFERENCES

(1) Geng, Z.; Li, Z.; Cui, Z.; Wang, J.; Yang, X.; Liu, C. Novel Bionic Topography with MiR-21 Coating for Improving Bone-Implant Integration through Regulating Cell Adhesion and Angiogenesis. *Nano Lett.* **2020**, *20*, 7716−7721.

(2) Young, J. L.; Hua, X.; Somsel, H.; Reichart, F.; Kessler, H.; Spatz, J. P. Integrin Subtypes and Nanoscale Ligand Presentation Influence Drug Sensitivity in Cancer Cells. *Nano Lett.* **2020**, *20*, 1183−1191.

(3) Senturk, B.; Cubuk, M. O.; Ozmen, M. C.; Aydin, B.; Guler, M. O.; Tekinay, A. B. Inhibition of VEGF Mediated Corneal Neovascularization by Anti-Angiogenic Peptide Nanofibers. *Biomaterials* **2016**, *107*, 124−132.

(4) Imanishi, J.; Kamiyama, K.; Iguchi, I.; Kita, M.; Sotozono, C.; Kinoshita, S. Growth Factors: Importance in Wound Healing and Maintenance of Transparency of the Cornea. *Prog. Retinal Eye Res.* **2000**, *19*, 113−129.

(5) Froger, N.; Matonti, F.; Roubeix, C.; Forster, V.; Ivkovic, I.; Brunel, N.; Baudouin, C.; Sahel, J.-A.; Picaud, S. VEGF Is an Autocrine/Paracrine Neuroprotective Factor for Injured Retinal Ganglion Neurons. *Sci. Rep.* **2020**, *10*, 12409.

(6) Chang, J.-H.; Garg, N. K.; Lunde, E.; Han, K.-Y.; Jain, S.; Azar, D. T. Corneal Neovascularization: An Anti-VEGF Therapy Review. *Surv. Ophthalmol.* **2012**, *57*, 415−429.

(7) Sullivan, L. A.; Brekken, R. A. The VEGF Family in Cancer and Antibody-Based Strategies for Their Inhibition. *mAbs* **2010**, *2*, 165−175.

(8) Fogli, S.; Del Re, M.; Rofi, E.; Posarelli, C.; Figus, M.; Danesi, R. Clinical Pharmacology of Intravitreal Anti-VEGF Drugs. *Eye* **2018**, *32*, 1010−1020.

(9) Qi, G.-B.; Gao, Y.-J.; Wang, L.; Wang, H. Self-Assembled Peptide-Based Nanomaterials for Biomedical Imaging and Therapy. *Adv. Mater.* **2018**, *30*, 1703444.

(10) Zhang, C.; Wu, W.; Li, R.-Q.; Qiu, W.-X.; Zhuang, Z.-N.; Cheng, S.-X.; Zhang, X.-Z. Peptide-Based Multifunctional Nanomaterials for Tumor Imaging and Therapy. *Adv. Funct. Mater.* **2018**, *28*, 1804492.

(11) Pepe-Mooney, B. J.; Fairman, R. Peptides as Materials. *Curr. Opin. Struct. Biol.* **2009**, *19*, 483−494.

(12) Hernandez-Garcia, A.; Álvarez, Z.; Simkin, D.; Madhan, A.; Pariset, E.; Tantakitti, F.; de J. Vargas-Dorantes, O.; Lee, S. S.; Kiskinis, E.; Stupp, S. I. Peptide−siRNA Supramolecular Particles for Neural Cell Transfection. *Adv. Sci.* **2019**, *6*, 1801458.

(13) Li, M.; Ning, Y.; Chen, J.; Duan, X.; Song, N.; Ding, D.; Su, X.; Yu, Z. Proline Isomerization-Regulated Tumor Microenvironment-Adaptable Self-Assembly of Peptides for Enhanced Therapeutic Efficacy. *Nano Lett.* **2019**, *19*, 7965−7976.

(14) Shang, Y.; Zhi, D.; Feng, G.; Wang, Z.; Mao, D.; Guo, S.; Liu, R.; Liu, L.; Zhang, S.; Sun, S.; Wang, K.; Kong, D.; Gao, J.; Yang, Z. Supramolecular Nanofibers with Superior Bioactivity to Insulin-Like Growth Factor-I. *Nano Lett.* **2019**, *19*, 1560−1569.

(15) Li, S.; Zhang, W.; Xing, R.; Yuan, C.; Xue, H.; Yan, X. Supramolecular Nanofibrils Formed by Coassembly of Clinically Approved Drugs for Tumor Photothermal Immunotherapy. *Adv. Mater.* **2021**, *33*, 2100595.

(16) Li, X.; Cai, X.; Zhang, Z.; Ding, Y.; Ma, R.; Huang, F.; Liu, Y.; Liu, J.; Shi, L. Mimetic Heat Shock Protein Mediated Immune Process to Enhance Cancer Immunotherapy. *Nano Lett.* **2020**, *20*, 4454−4463.

(17) Ji, W.; Yuan, C.; Chakraborty, P.; Makam, P.; Bera, S.; Rencus-Lazar, S.; Li, J.; Yan, X.; Gazit, E. Coassembly-Induced Transformation of Dipeptide Amyloid-Like Structures into Stimuli-Responsive Supramolecular Materials. *ACS Nano* **2020**, *14*, 7181−7190.

(18) Carlini, A. S.; Choi, W.; McCallum, N. C.; Gianneschi, N. C. pH-Responsive Charge-Conversion Progelator Peptides. *Adv. Funct. Mater.* **2021**, *31*, 2007733.

(19) Hu, X.-X.; He, P.-P.; Qi, G.-B.; Gao, Y.-J.; Lin, Y.-X.; Yang, C.; Yang, P.-P.; Hao, H.; Wang, L.; Wang, H. Transformable Nanomaterials as an Artificial Extracellular Matrix for Inhibiting Tumor Invasion and Metastasis. *ACS Nano* **2017**, *11*, 4086−4096.

(20) He, P.-P.; Li, X.-D.; Fan, J.-Q.; Fan, Y.; Yang, P.-P.; Li, B.-N.; Cong, Y.; Yang, C.; Zhang, K.; Wang, Z.-Q.; Hou, D.-Y.; Wang, H.; Wang, L. Live Cells Process Exogenous Peptide as Fibronectin Fibrillogenesis *in Vivo*. *CCS Chemistry* **2020**, *2*, 539−554.

(21) Chen, Z.; Zhang, K.; Fan, J.; Fan, Y.; Yang, C.; Tian, W.; Li, Y.; Li, W.; Zhang, J.; Wang, H.; Wang, L. *In Situ* Construction of Ligand Nano-Network to Integrin $\alpha_v\beta_3$ for Angiogenesis Inhibition. *Chin. Chem. Lett.* **2020**, *31*, 3107−3112.

(22) Wen, S.; Zhang, K.; Li, Y.; Fan, J.; Ziming, C.; Zhang, J.; Wang, H.; Wang, L. A Self-Assembling Peptide Targeting VEGF Receptors to Inhibit Angiogenesis. *Chin. Chem. Lett.* **2020**, *31*, 3153−3157.

(23) Robinson, S. D.; Hodivala-Dilke, K. M. The Role of β_3-Integrins in Tumor Angiogenesis: Context Is Everything. *Curr. Opin. Cell Biol.* **2011**, *23*, 630−637.

(24) Kumar, C. C. Integrin $\alpha_v\beta_3$ as a Therapeutic Target for Blocking Tumor-Induced Angiogenesis. *Curr. Drug Targets* **2003**, *4*, 123−131.

(25) Oliveira, C. R. d.; Marqueti, R. d. C.; Cominetti, M. R.; Douat, E. S. A. V.; Ribeiro, J. U.; Pontes, C. L. S.; Borghi-Silva, A.; Selistre-de-Araujo, H. S. Effects of Blocking Alpha(v)beta(3) Integrin by a Recombinant RGD Disintegrin on Remodeling of Wound Healing after Induction of Incisional Hernia in Rats. *Acta Cir. Bras.* **2015**, *30*, 134−142.

(26) Klotz, O.; Park, J. K.; Pleyer, U.; Hartmann, C.; Baatz, H. Inhibition of Corneal Neovascularization by α_v-Integrin Antagonists in the Rat. *Graefe's Arch. Clin. Exp. Ophthalmol.* **2000**, *238*, 88−93.

(27) Koutsioumpa, M.; Polytarchou, C.; Courty, J.; Zhang, Y.; Kieffer, N.; Mikelis, C.; Skandalis, S. S.; Hellman, U.; Iliopoulos, D.; Papadimitriou, E. Interplay between $\alpha_v\beta_3$ Integrin and Nucleolin Regulates Human Endothelial and Glioma Cell Migration. *J. Biol. Chem.* **2013**, *288*, 343−354.

(28) Choi, Y.; Kim, E.; Lee, Y.; Han, M. H.; Kang, I.-C. Site-Specific Inhibition of Integrin $\alpha_v\beta_3$-Vitronectin Association by a Ser-Asp-Val Sequence through an Arg-Gly-Asp-Binding Site of the Integrin. *Proteomics* **2010**, *10*, 72−80.

(29) Rzepecki, P.; Schrader, T. β-Sheet Ligands in Action: KLVFF Recognition by Aminopyrazole Hybrid Receptors in Water. *J. Am. Chem. Soc.* **2005**, *127*, 3016−3025.

(30) Mana, G.; Clapero, F.; Panieri, E.; Panero, V.; Böttcher, R. T.; Tseng, H.-Y.; Saltarin, F.; Astanina, E.; Wolanska, K. I.; Morgan, M. R.; Humphries, M. J.; Santoro, M. M.; Serini, G.; Valdembri, D. PPFIA1 Drives Active $\alpha5\beta1$ Integrin Recycling and Controls Fibronectin Fibrillogenesis and Vascular Morphogenesis. *Nat. Commun.* **2016**, *7*, 13546.

(31) Van Agthoven, J. F.; Xiong, J.-P.; Alonso, J. L.; Rui, X.; Adair, B. D.; Goodman, S. L.; Arnaout, M. A. Structural Basis for Pure Antagonism of Integrin $\alpha_V\beta_3$ by a High-Affinity Form of Fibronectin. *Nat. Struct. Mol. Biol.* **2014**, *21*, 383−388.

(32) Xu, A. P.; Yang, P. P.; Yang, C.; Gao, Y. J.; Zhao, X. X.; Luo, Q.; Li, X. D.; Li, L. Z.; Wang, L.; Wang, H. Bio-Inspired Metal Ions Regulate the Structure Evolution of Self-Assembled Peptide-Based Nanoparticles. *Nanoscale* **2016**, *8*, 14078−14083.

(33) Niu, L.; Liu, L.; Xu, M.; Cramer, J.; Gothelf, K. V.; Dong, M.; Besenbacher, F.; Zeng, Q.; Yang, Y.; Wang, C. Transformation of β-Sheet Structures of the Amyloid Peptide Induced by Molecular Modulators. *Chem. Commun.* **2014**, *50*, 8923−8926.

(34) Castelletto, V.; Hamley, I. W.; Harris, P. J. F.; Olsson, U.; Spencer, N. Influence of the Solvent on the Self-Assembly of a Modified Amyloid Beta Peptide Fragment. I. Morphological Investigation. *J. Phys. Chem. B* **2009**, *113*, 9978−9987.

(35) Kireeva, M. L.; Lam, S. C. T.; Lau, L. F. Adhesion of Human Umbilical Vein Endothelial Cells to the Immediate-Early Gene Product Cyr61 Is Mediated through Integrin $\alpha_v\beta_3$. *J. Biol. Chem.* **1998**, *273*, 3090−3096.

(36) Guo, Z.; He, B.; Jin, H.; Zhang, H.; Dai, W.; Zhang, L.; Zhang, H.; Wang, X.; Wang, J.; Zhang, X.; Zhang, Q. Targeting Efficiency of RGD-Modified Nanocarriers with Different Ligand Intervals in Response to Integrin $\alpha_v\beta_3$ Clustering. *Biomaterials* **2014**, *35*, 6106−6117.

(37) Zhang, Z.; Ma, J.-x.; Gao, G.; Li, C.; Luo, L.; Zhang, M.; Yang, W.; Jiang, A.; Kuang, W.; Xu, L.; Chen, J.; Liu, Z. Plasminogen Kringle 5 Inhibits Alkali-Burn−Induced Corneal Neovascularization. *Invest. Ophthalmol. Visual Sci.* **2005**, *46*, 4062−4071.

https://doi.org/10.1021/acsnano.1c02194
ACS Nano 2021, 15, 13065−13076

(38) Beriault, D. R.; Werstuck, G. H. Detection and Quantification of Endoplasmic Reticulum Stress in Living Cells Using the Fluorescent Compound, Thioflavin T. *Biochim. Biophys. Acta, Mol. Cell Res.* **2013**, *1833*, 2293−2301.

https://doi.org/10.1021/acsnano.1c02194
ACS Nano 2021, 15, 13065−13076